CHEMISTRY OF MATERIALS

pubs.acs.org/cm

Article

Radical-Enriched Artificial Melanin

Wei Cao, Alex J. Mantanona, Haochuan Mao, Naneki C. McCallum, Yang Jiao, Claudia Battistella, Valeria Caponetti, Nanzhi Zang, Matthew P. Thompson, Marco Montalti, J. Fraser Stoddart, Michael R. Wasielewski, Jeffrey D. Rinehart,* and Nathan C. Gianneschi*

Cite This: *Chem. Mater.* 2020, 32, 5759–5767

Read Online

ACCESS | Metrics & More | Article Recommendations | Supporting Information

ABSTRACT: Melanin is a class of ubiquitous, heterogeneous, polymeric pigments. One of the most unusual features of melanin is the presence of stable persistent radicals, which has been reported to relate to ionizing radiation protection, including X-rays and gamma rays. In this work, we aimed to increase the radical content by introducing nitroxide radicals into synthetic melanin nanomaterials. Nanoparticles (NPs) were prepared by copolymerization of a stable radical modified monomer with the monomer dopamine. The radical content increased to 1 order of magnitude higher than that of the conventional melanin-like material, polydopamine. These radical NPs can enter human epidermal keratinocytes and form perinuclear caps, mimicking natural melanin synthesized by melanocytes. We demonstrated that these NPs display protective properties by scavenging reactive oxygen species, one of the most important biological effects of ionizing radiation exposure. This finding may have potential application for materials capable of mitigating side effects of clinical radiation therapy.

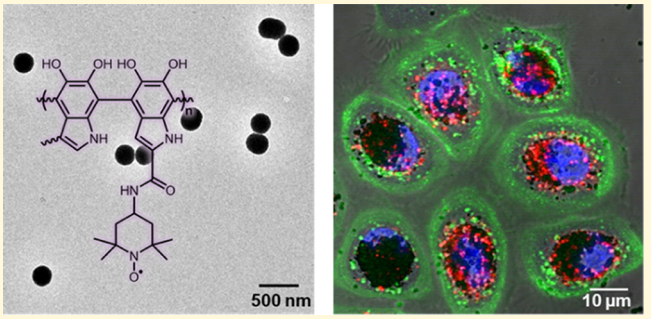

INTRODUCTION

Melanins are a collection of biological pigments with unusual physicochemical properties existing ubiquitously in biology.[1−4] They provide coloration, social communication, free radical scavenging, and photo protection among other applications.[5−15] Understanding melanin and melanogenesis has been a long standing biomaterials problem.[16] A core aspect of these findings is that melanin function is closely related to its heterogeneous structure.[2] One of the most unusual features of the structural biology of melanin biopolymers is its persistent electron paramagnetic resonance (EPR) signal. In fact, melanin was among the first biological materials examined by EPR spectroscopy.[17] Melanin consists of intrinsic indole semiquinone-like doublet-state radicals, which originate from an equilibrium between quinone and hydroquinone to yield semiquinone.[5,18,19] The radicals are the catalytic centers for superoxide decomposition[11] and can be utilized to determine the ratio between the two main types of mammalian melanin pigments: pheomelanin and eumelanin.[20]

Developing radioprotective nanomaterials is of importance for myriad applications. To avoid occupational hazards from ionizing radiation exposure, researchers traditionally use heavy metals or their composites to attenuate radiation.[21] However, issues of heaviness or bulkiness hamper their attractiveness as ideal candidates for radiation protection. Radiotherapy is an important treatment modality for many cancers with as many as 60% of cancer patients receiving ionizing radiation.[22] The toxicity and side effects associated with radiation can significantly affect quality of life;[23,24] thus, the development of protectors is attractive.[21,25] In addition, due to the intrinsic large surface-area-to-volume ratio, nanoparticles have been reported to enhance the absorption of high-energy photons.[26]

Melanin is used in nature as a nanoscale radiation protector.[27−29] For example, melanized fungi were found to have colonized the walls and the cooling pool water at the Chernobyl nuclear reactor site.[30] Further studies showed that melanized *Cryptococcus neoformans* grew better with high doses of gamma-ray radiation than without, provocatively indicating their "radiotrophic" nature.[27] In addition, prior research has shown that melanin can protect animal models from the deadly effects of high doses of X-rays or gamma-ray radiation.[31] Dadachova et al. performed Monte Carlo simulations, which indicated that, by increasing the radical content in melanin, the attenuation of X-rays should be enhanced.[32] The mechanism relies on the trapping of Compton recoil electrons by free radicals in melanin. Unfortunately, the scale of radical content of the materials used in these previous studies has been limited, which may in turn limit their scope of effective protection.

Received: April 13, 2020
Revised: June 13, 2020
Published: July 2, 2020

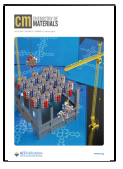

https://dx.doi.org/10.1021/acs.chemmater.0c01573
Chem. Mater. 2020, 32, 5759–5767

The intrinsic radical content in natural and synthetic melanin is low. It has been suggested that transition-metal coordination chemistry could be employed to tune the radical content.[33] An early EPR study indicated that paramagnetic metal ions like copper(II) could quench the melanin EPR signal,[34] while other researchers showed that coordination of diamagnetic, multivalent metal ions like zinc(II) and cadmium-(II) led to a marked increase in the intensity of the EPR signal.[35] However, inclusion of heavy metals generally raises concerns in biomedical applications of materials and molecules. Therefore, in this study, we aimed to develop a metal-free methodology to manipulate the radical content of melanin. (2,2,6,6-Tetramethylpiperidin-1-yl)oxyl (TEMPO) is one of the most commonly used bench stable free radicals.[36] Its derivatives such as 4-hydroxy-2,2,6,6-tetramethylpiperidine-*N*-oxyl (TEMPOL) have been used for scavenging reactive oxygen species (ROS) as supplements for human health.[5,37,38] We hypothesized that, by introducing more stable radicals into synthetic melanin, we could enhance the X-ray protection properties of the resulting artificial melanin nanoparticles. This was tested by preparing radical-enriched melanin nanoparticles by copolymerization of a conventional dopamine monomer **1** with a radical-labeled monomer **2** (Figure 1). The resulting particles have altered electrochemical and magnetic properties compared with polydopamine-based synthetic melanin. The radical NPs readily form perinuclear caps in neonatal human epidermal keratinocytes (NHEKs) and can efficiently quench the reactive oxygen species generated by X-ray irradiation.

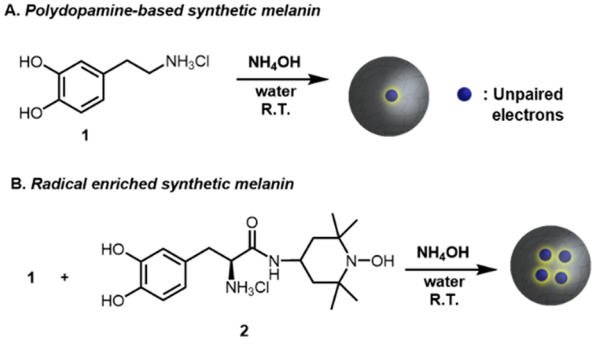

Figure 1. Radical-enriched melanin. (A) Polydopamine-based synthetic melanin nanoparticles, referred to "PDA NPs". (B) Copolymerization of dopamine with radical monomers generates radical-enriched melanin nanoparticles, referred to herein as "radical NPs".

EXPERIMENTAL SECTION

Materials and Instrumentation. See the Supporting Information for complete descriptions of instrumentation, materials, and general procedures.

Synthesis of Radical-Enriched Materials. In a typical experiment for 3:1 NPs,[9] monomer **2** (18 mg, 0.05 mmol) was dissolved in 12 mL of MilliQ water and transferred to a clean round bottom flask. Monomer **1** (30 mg, 0.16 mmol) was then added to the solution. Two milliliters of ethanol and 63 μL of ammonium hydroxide were added to the reaction flask under vigorous stirring. The reaction was exposed to air and stirred at room temperature for 24 h. For purification, the dark brown to black melanin samples were centrifuged at 11,000 rpm for 10 min followed by washing with MilliQ water three times. The mass concentration of the melanin solution was determined by lyophilizing a known volume of the final solution overnight and then weighing the sample.

Radical Content Measurement. EPR experiments were performed in a quartz capillary (i.d. of 1.50 mm and o.d. of 1.80 mm). A water suspension of melanin NPs was added to the capillary to the same height. Continuous wave EPR spectra were collected at X-band (9.5 GHz) fields using a Bruker Elexsys E680 spectrometer equipped with a 4122SHQE resonator. Scans were performed with a magnetic field modulation amplitude of 2 G and non-saturating microwave power of 1.544 mW. The results are the average of 32 scans.

Magnetic data was collected on a Quantum Design magnetic properties measurements system 3 (MPMS3) superconducting quantum interference device (SQUID) magnetometer in the direct current scan mode with a maximum field of 7 T. Magnetic measurements were performed on freeze-dried solid samples (~5 mg) pressed into standard Quantum Design plastic sample holders to prevent torqueing. All data was corrected for diamagnetism using Pascal's constants.[39]

Cell Viability. Primary NHEK cells were isolated from freshly excised neonatal foreskins and gifted by the Perez-White lab at Northwestern Feinberg School of Medicine. An M154 medium supplemented with human keratinocyte growth supplement (HKGS), 10 μg/mL gentamicin, 0.25 μg/mL amphotericin B, and 0.07 mM $CaCl_2$ was used to incubate the cells. HeLa cells were cultured in Dulbecco's modified Eagle medium (DMEM) supplemented with 10% fetal bovine serum (FBS) and 1% penicillin–streptomycin. All cells were maintained at 37 °C and 5% CO_2 with a relative humidity of 95%. HeLa cells were plated in 96-well plates at a density of 10k/well and then incubated at 37 °C with 5% CO_2 for 24 h. The cells were then treated with NPs for the desired time followed by washing three times with phosphate-buffered saline (PBS). Then, 20 μL of a CellTiter-Blue reagent in 200 μL of medium was added to each well and incubated for 2–3 h to allow the live cells to convert resazurin to fluorescent resorufin. The cells were shaken for 10 s before the fluorescent signal was analyzed by the plate reader with an excitation wavelength at 560 nm and emission wavelength at 600 nm. Five replicates were performed for each independent sample; 10% DMSO was used as a negative control, and pure medium was used as a positive control.

X-ray Experiments. Cells were irradiated using a Radsource RS-2000 X-ray irradiator at a dose rate of 4.4 Gy/min. Lead sheets were used to shield the X-rays. Gray (Gy) is defined as the absorption of one joule of radiation energy per kilogram of matter. 1 Gy = 1 J/kg.

Mediated Electrochemical Probe Experiments. Mediated electrochemical probing experiments were carried out on a Gamry Multipurpose instrument. A standard three-electrode system was employed with a gold electrode as the working electrode. We followed literature methods to prepare the melanin-loaded working electrode.[40,41] Briefly, chitosan was first dissolved in pH = 5.5 HCl solution at 10 mg mL^{-1} under sonication. Then, 5 μL of melanin solution was mixed with 20 μL of chitosan solution and drop-casted onto a polished gold electrode. After drying under vacuum for 1 h, the chitosan film was rinsed carefully with 100 mM PBS to neutralize the chitosan, yielding a relatively stable chitosan hydrogel film on the electrode due to the solubility difference of chitosan in different pH environments. The Ag/AgCl electrode was the reference electrode, and the counter electrode was a Pt coil. Argon was continuously purged gently in the cell during the experiment. Three mediators were used: 50 μM 1,1′-ferrocenedimethanol, 100 μM potassium hexaammineruthenium(III) chloride, and 50 μM hexaamine ruthenium-(III). These were dissolved in 100 mM phosphate buffered saline (PBS) solution (10× PBS) and prepared fresh. The scan rate was kept at 50 mV/s.

Reactive Oxygen Species (ROS) Scavenging in NHEK Cells. NHEK cells were sourced as stated above and plated in a four-chamber glass bottom confocal dish at 15,000 cells/chamber. After 24 h of incubation to allow the cells to attach, 0.04 mg mL^{-1} nanoparticles were added to the cells. Following incubation for another 24 h, cells were washed three times with 500 μL of DPBS to remove the free NPs in the medium. Cells were treated with 0.8 μM 2′,7′–dichlorofluorescein diacetate (DCFDA) in DPBS solution and

https://dx.doi.org/10.1021/acs.chemmater.0c01573
Chem. Mater. 2020, 32, 5759–5767

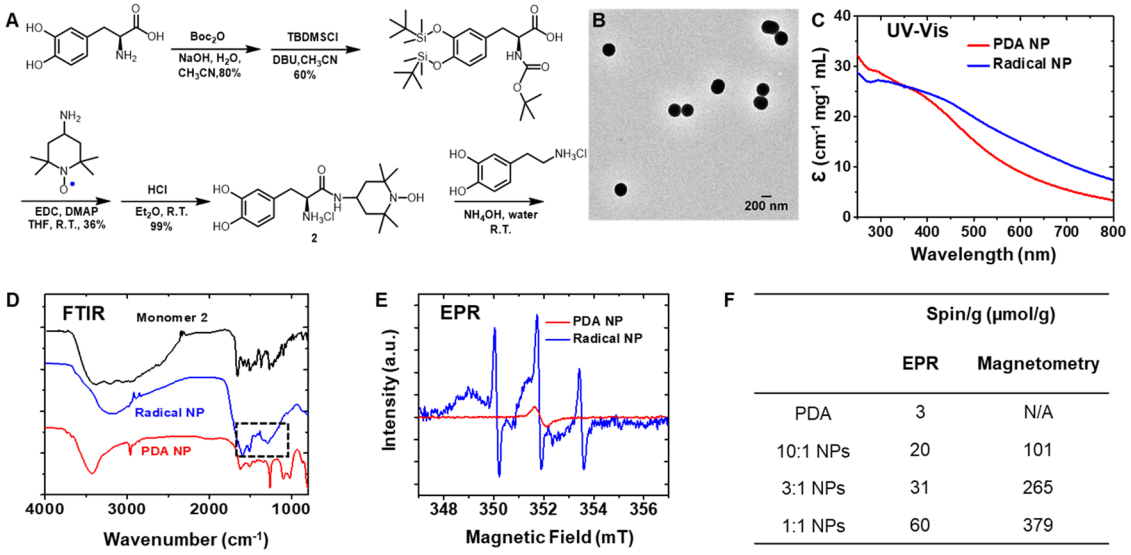

Figure 2. Synthesis and characterization of the radical nanoparticles. (A) Synthetic route of the monomer **2** and radical NPs. (B) TEM image of the 3:1 radical NP. (C) Extinction coefficient comparison of the 3:1 radical NP and the PDA NP. (D) FTIR spectra of monomer **2**, 3:1 radical NP, and PDA NP. (E) EPR spectra of the 3:1 radical NP measured in aqueous suspension overlaid with the EPR spectrum of PDA NP. (F) Spin concentrations in the different radical NPs quantified by EPR spectroscopy and SQUID magnetometry.

incubated at 37 °C for 20 min. The loading buffer was removed, and the cells were returned to the growth medium. Then, the cells were irradiated with 2 Gy X-ray irradiation. A drop of Hoechst 33342 dye was added for nucleus staining before imaging by confocal laser scanning microscopy (CLSM). Live cells were imaged on a Leica SP5 confocal microscope with a smart gain of 70% and laser power of 12%.

ROS probe scan excitation wavelength: 488 nm; detection wavelength: 510−550 nm. Hoechst 33342 (nuclear) scan excitation wavelength: 405 nm; detection wavelength: 420 to 480 nm.

For quantification analysis of confocal laser scanning microscopy images, the area within the cell was selected by thresholding the filtered green channel (Gaussian blur). The resulting area was applied to the original channel as a region of interest. Then, mean fluorescence intensities were analyzed by Image J.

Intracellular Distribution of NPs in NHEK Cells by CLSM. NHEK cells were treated with NP suspensions for 24 h. The cells were stained with 5 μg/mL wheat germ agglutinin (WGA) conjugated to Alexa Fluor 488 in DPBS for 10 min at room temperature, washed with PBS, and returned to the complete growth medium. Before confocal microscopy imaging, Hoechst 33342 dye and LysoTracker red stock solution (final concentration: 75 nM) were added to stain the nuclei and lysosomes, respectively. No further washing or fixation was employed before imaging, as LysoTracker red is sensitive to photobleaching. Confocal microscopy was employed to observe the cell uptake and distribution.

WGA 488 (membrane) scan excitation wavelength: 488 nm; detection wavelength: 510−550 nm. Hoechst 33342 (nuclear) scan excitation wavelength: 405 nm; detection wavelength: 420−480 nm. Lysotracker red (lysosome) scan excitation wavelength: 561 nm; detection wavelength: 585−649 nm.

RESULTS AND DISCUSSION

Radical-Enriched Melanin Nanoparticles. The radical-enriched melanin was synthesized by copolymerization of radical monomer **2** with the conventional monomer, dopamine hydrochloride **1** (Figure 2). Monomer **2** was synthesized by amide coupling of 3-(3,4-dihydroxyphenyl)-L-alanine (L-DOPA) with 4-amino-TEMPO similar to a previous procedure[42] (Figure 2A).

L-DOPA was chosen to generate radical-enriched synthetic melanins instead of dopamine as it could be functionalized on the carboxylic acid without blocking the polymerizable catechol and amine functional groups while retaining much of the character of the dopamine-based system. To begin with, the amine group and catechol of L-DOPA were protected using Boc anhydride and *tert*-butyldimethylsilyl chloride (TBDMSCl), respectively. The amide coupling reaction was then performed followed by deprotection to give monomer **2** as a white powder in a 20% overall yield. The nitroxide radical of the TEMPO moiety was reduced to its corresponding hydroxylamine derivative during the deprotection process, which eliminated the interference of paramagnetic radical species with magnetic fields, therefore allowing clear NMR spectra to be obtained in methanol-d_4 (Figures S1 and S2).

With monomer **2** in hand, we embarked on the synthesis of NPs by a chemical oxidation approach. Although the reactions yielded dark suspensions (Figure S3) suggesting successful polymerization, it was difficult to obtain regularly shaped nanostructures. The irregular aggregates formed by small particles indicated to us that the reaction kinetics were too fast for clean NP synthesis (Figure S3). To slow down the reaction, copolymerization of dopamine **1** with monomer **2** (molar ratio of 3:1) was performed under alkaline conditions using ammonium hydroxide, which also enabled regeneration of nitroxide radical on the TEMPOH moiety of monomer **2** (Figure S4). The reaction yielded uniform spherical nanoparticles with a hydrodynamic radius of ∼180 nm. The spherical morphology of the NPs (referred to as radical NPs) was confirmed by transmission electron microscopy (TEM) analysis without staining (Figure 2B and Figure S5 for additional TEM images). Other oxidative agents such as sodium periodate and potassium permanganate and bases such as potassium hydroxide and tris(hydroxymethyl)-aminomethane buffer were also screened but did not yield uniform morphologies. Attempts to copolymerize L-DOPA with monomer **2** did not yield uniform nanostructures either, the reason for which remains elusive to us. However, our nanoparticle synthesis strategy does not involve any organic solvents, heating, or harsh conditions, making it a clean method for preparing these functionalized melanin materials.

https://dx.doi.org/10.1021/acs.chemmater.0c01573
Chem. Mater. 2020, 32, 5759−5767

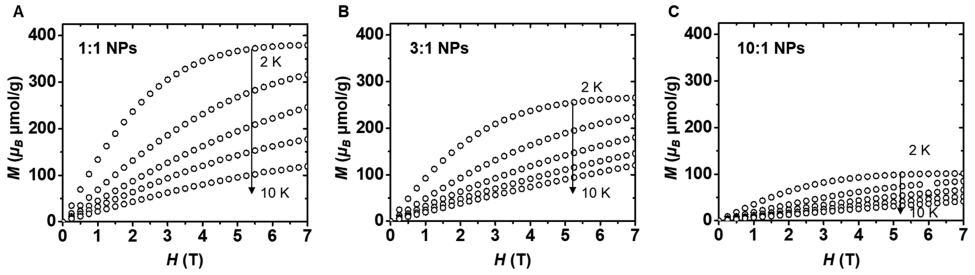

Figure 3. Magnetization vs magnetic field plots performed at various temperatures for (A) 1:1, (B) 3:1, and (C) 10:1 NPs. Saturation values at 2 K and 7 T were used to calculate the radical concentration.

Note that previous literature reports utilize monomer **2** as a surface coating on planar substrates[42,43] and polymeric microspheres.[44] Our work here focuses on the polymerization of monomer **2** in solution for radical-enriched melanin nanoparticles.

We followed the time evolution of polymerization using UV−vis spectroscopy. The kinetics of radical melanin polymerization were much faster than those of polydopamine synthesis using pure dopamine hydrochloride as the only monomer (Figure S6). The quenched TEMPOH is capable of generating free radicals in the presence of ammonium hydroxide (Figure S4), and it has been reported that TEMPO can catalyze the oxidation of phenols and alcohols,[45] which is the rate-determining step for the auto-polymerization of dopamine.[10] Therefore, we attribute the significant acceleration of NP formation to the presence of the TEMPO moiety. We suspect that the altered reaction kinetics may provide a control point for the chemical structures of polydopamine.[46] To probe whether the structure of radical-enriched melanin changed in comparison to PDA NPs, we measured the extinction coefficients of the particles. From Figure 2C, the extinction coefficient is higher in the long-wavelength range (>350 nm). Since melanins are known to consist of monomers covalently combined in a variety of oligomers that in turn assemble[47] contributing to the broad absorption spectra, the extinction coefficient comparison suggests that long oligomer/polymers are formed in the TEMPO-catalyzed reaction.[47]

Mass spectrometry studies suggested that polymerization of monomer **2** occurred via a 5,6-dihydroxyindole-2-carboxylic acid (DHICA) pathway (Figures S7 and S8). 5,6-Dihydroxyindole (DHI) exhibits more efficient π-conjugation than DHICA melanin.[48] Monomer **2** is a functionalized analogue of L-DOPA. We anticipate that, in radical NPs, the atropisomerism arises because a hindered rotation of the dihydroxyindole-type moiety of monomer **2** would be stronger than that of typical DHICA melanin. As demonstrated by Li and co-workers,[49] the interrupted nonplanar structure could potentially lead to greater antioxidant properties.

Characterization of Nanoparticles. The co-polymerization of dopamine and L-DOPA-TEMPOH was confirmed by Fourier-transform infrared (FTIR) and EPR spectra (Figure 2D,E). Absorption peaks around 1600, 1510, and 1294 cm^{-1} were ascribed to the amide bond vibration from monomer **2**. The UV−vis spectrum (Figure 2C) of the sample after purification by multiple rounds of centrifugation showed the typical monotonic broad band absorption, which also confirmed the success of dopamine polymerization. EPR enables a sensitive and nondestructive way to analyze the radical species in melanin. The three distinct lines in the EPR spectrum (Figure 2E) suggest that nitroxide radicals are incorporated in the final NPs. Considering the versatility of amide chemistry, this method could potentially be used to create a vast array of functional melanin materials.

With the copolymerization methodology verified, we prepared a library of NPs with different radical contents by varying the feeding ratio of dopamine and monomer **2**. NPs were prepared at 10:1, 3:1, and 1:1 molar ratios of dopamine versus monomer **2** (Figure 2F), and the radical content was evaluated by quantitative EPR using a 4-amino-TEMPO aqueous solution as the standard (Figures S9−S11). The radical content of conventional PDA was approximately 3 μmol/g, which is consistent with previous reports.[32] For the 3:1 NPs, the radical content was 31 μmol/g with the 1:1 NPs measured at 60 μmol/g. The 10:1, 3:1, and 1:1 NPs represent the feeding ratio of the dopamine to monomer **2** and may not correlate with the final composition in the particles as a detailed EPR study suggested that some hydroxylamine derivative of monomer **2** is present in the radical NPs (Figures S12 and S13). As shown in both EPR and magnetometry data (Figure S14), the spin concentration increases with an increase in the ratio of monomer **2**. This suggests that the incorporation of monomer **2** in the radical-enriched material is consistent as we increase the monomer concentration. Using our copolymerization strategy, we increased the radical content by more than an order of magnitude as compared to conventional PDA. The radical signals are highly stable and remain intact after a high dosage of X-ray radiation (Figure S15). Notably, the three line EPR spectra of our radical NP material due to the hyperfine splitting of nitrogen are intrinsically different from those of the reported PDA,[33] poly(L-DOPA),[50] DHN-type allomelanin,[29] or other natural melanin examples.[20]

SQUID magnetometry can provide a useful comparison to EPR data as it is sensitive to all sources of magnetic moment whereas EPR is sensitive to specific magnetic transitions. This sensitivity, however, makes the diamagnetic contribution of the NP on par with the radical paramagnetism, thus limiting magnetic analysis to low temperatures (T < 30 K). Direct current field-dependent measurements (Figure 3) were used to estimate the radical content at low temperatures. Radical content was calculated with the saturated magnetic moment of each sample at 2 K representing the sum of paramagnetic contributions from S = 1/2 radicals and reported as Bohr magnetons (μ_B) per gram of average monomer unit. The calculated values were an order of magnitude larger than the values found through EPR (Figure 2F). This discrepancy may be due to a variety of factors including slight differences in the EPR standard and the sample shape, dielectric constant, and transition probabilities.[51] It may also be potentially due to the radical concentration within the NP leading to significant

https://dx.doi.org/10.1021/acs.chemmater.0c01573
Chem. Mater. 2020, 32, 5759−5767

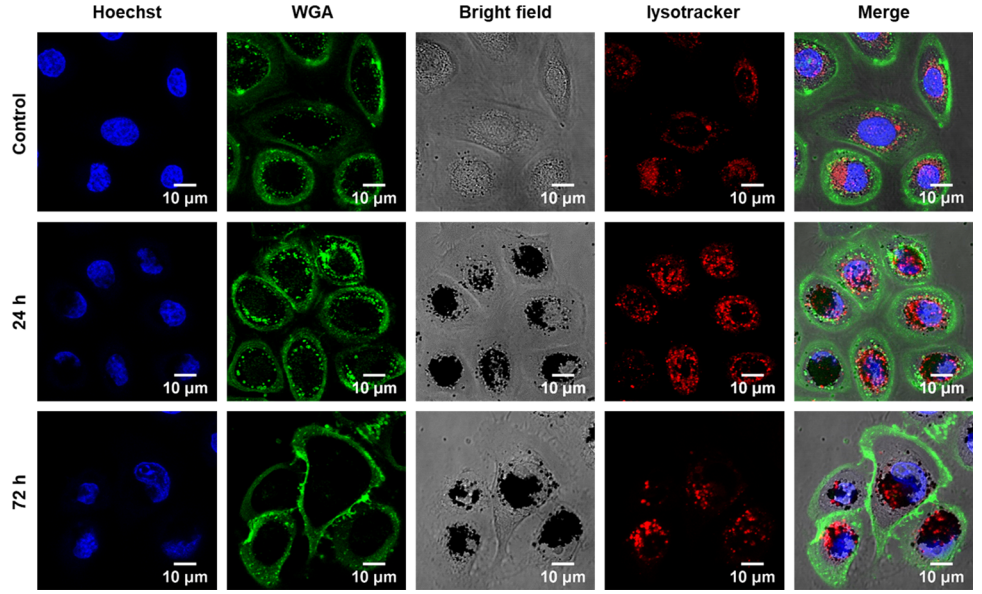

Figure 4. Live-cell confocal microscopy of NHEK cells after incubating radical NPs for 24 or 72 h or without NP treatment. The cells were plated in a glass-bottom, four-chamber dish, incubated with NPs for desired periods of time, and then stained with wheat germ agglutinin (WGA) conjugated to Alexa Fluor 488 (Ex 488 nm, false color: green), LysoTracker Red (Ex 561 nm, false color: red), and Hoechst 33342(Ex 405 nm, false color: blue).

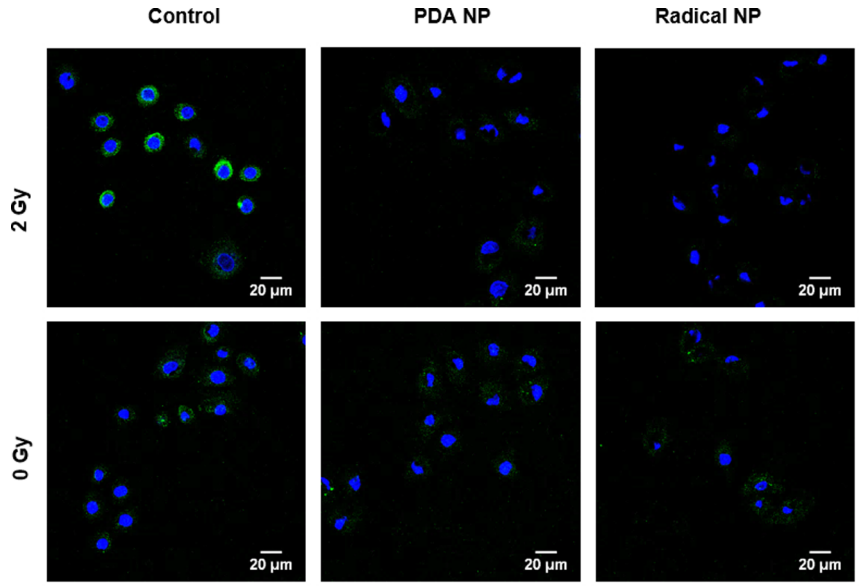

Figure 5. ROS scavenging in NHEK cells observed by live-cell confocal microscopy using an ROS-responsive DCFDA probe (Ex 488 nm, false color green). Untreated, X-ray-irradiated cells show a higher ROS signal. Nuclei were stained with Hoechst 33342 dye (Ex 405 nm, false color: blue).

signal broadening for some fraction of the radicals. Although the exact cause for this discrepancy is unknown, the trend for the radical concentration is consistent with the EPR data with increases in the solid-state radical concentration being roughly the same magnitude as the increases in the solution-state quantification. This trend did not increase in a linear fashion with an increase in the TEMPO monomer concentration, an observation which could have a chemical origin or be a manifestation of antiferromagnetic interactions at high radical concentrations as previously observed in Fe-PDA and other TEMPO-containing polymers.[52,53] Further corroboration is required to determine the origin of this behavior as the weak magnetic susceptibility does not permit collection of high-temperature magnetic susceptibility data, which would confirm or deny the presence of coupled spins.

Biocompatibility and Intracellular Distribution. To assess biological interactions of radical NPs in cells, the materials were tested in NHEK and HeLa cells. We selected the 3:1 NPs for these investigations as they contained a higher radical content than the 10:1 NPs and they were not observed to aggregate just as with the 1:1 NPs. Cell viability was assessed using the CellTiter-Blue assay, and even at high concentrations up to 0.2 mg mL^{-1} radical NPs, cells remained viable, indicating potential biocompatibility (Figure S16). We then explored the time-dependent uptake of NPs by CLSM. After a 1 h incubation of NHEK cells with 0.005 mg mL^{-1}

https://dx.doi.org/10.1021/acs.chemmater.0c01573
Chem. Mater. 2020, 32, 5759−5767

radical NPs, we were able to detect the uptake of the materials and initial delivery to the perinuclear region, albeit in a random distribution around the nucleus (Figure S17). After 24 h of incubation, perinuclear caps formed on one or both ends of the nuclei, mimicking the naturally asymmetric perinuclear melanin distribution in human keratinocyte cells. Cell pellets formed during centrifugation were light brown to black in color depending on the NP concentrations (Figures S18 and S19). We attribute this to the broad band absorption of the NPs across the UV−vis range (Figure 2C), indicating uptake of the radical NPs into the cells. In each case, we observed >99% uptake (and virtually every cell incorporated the radical NPs), and there were no differences in cell morphology compared with untreated control cells under the conditions studied as determined by confocal microscopy.

To further explore the cellular fate of radical NPs, staining techniques were employed for better visualization and mechanistic information. Wheat germ agglutinin is a lectin that can selectively bind with *N*-acetyl-D-glucosamine on the cell membrane. Alexa Fluor 488-conjugated WGA was used to stain the cell membrane, and Lysotracker red was used to probe the NP uptake pathway (Figure 4). The CLSM images suggested co-localization of the signal originating from the black NPs in the bright field images, and the red signal from the Lysotracker channel. Pearson's co-localization coefficient was determined to be 0.36 for 24 h images and 0.25 for 72 h images, which indicates weak co-localization. However, we note that bright field imaging hinders this analysis. Nevertheless, the confocal images suggest a lysosomal uptake pathway, consistent with that of natural melanin.[12,54]

Reactive Oxygen Species Scavenging. Ionizing radiation exposure triggers the accumulation of reactive oxygen species (ROS) and destroys the metabolic redox balance in cells. ROS accounts for two thirds of the radiobiological effects.[55] Hence, we investigated the ROS scavenging properties of cells treated with radical NPs and exposed to X-ray irradiation. NHEK cells were loaded with an ROS-responsive fluorogenic probe, DCFDA, prior to X-ray irradiation and then imaged by CLSM. DCFDA is a cell-permeable fluorogenic probe suitable for detecting intracellular ROS induced by X-ray irridiation.[56] Elevated turn-on green fluorescence was observed after 2 Gy X-ray irradiation in the control group with no NP treated cells (Figure 5 and Figures S20 and S21), which is consistent with previous reports.[57] For the radical melanin or PDA (0.04 mg mL^{-1})-treated cells, no fluorescence from the ROS probe was observed, indicating that our materials are efficient ROS scavengers in NHEK cells. Quantification of the mean fluorescence intensity of the ROS probe (Figure S22) also agrees with this statement.

The ROS scavenging ability of materials is closely related to their redox properties. To directly compare the redox properties of radical NPs with PDA NPs, we utilized mediated electrochemical probing experiments based on a method reported by Payne and co-workers.[40,41] To conduct these studies, the particles were first immobilized on a gold working electrode. This was achieved by imbedding the radical NPs and PDA NPs in a chitosan hydrogel film formed on the gold electrode, utilizing the pH-dependent solubility of chitosan. The electrode was then immersed in a 100 mM PBS solution containing three redox mediators (50 μM 1,1′-ferrocenedimethanol, 100 μM potassium hexachloroiridate (III), and 50 μM hexaammineruthenium (III) chloride). The cyclic voltammetry (CV) curves were plotted in comparison to a blank chitosan film (Figure 6). For the control chitosan films, a small current was observed due to the difficult diffusion of mediators

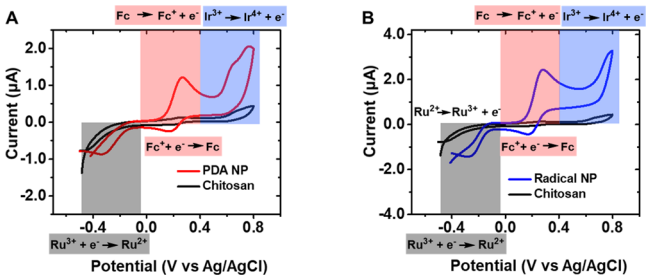

Figure 6. Mediated electrochemical probing experiments to compare the redox behavior of radical and PDA NPs. Cyclic voltammograms of chitosan hydrogel films with (A) PDA NPs (red plot) and (B) radical NPs (blue plot) encapsulated in comparison to the control of blank chitosan film (black plot) (a scan rate of 50 mV/s) in the presence of three different redox mediators (1,1′-ferrocenedimethanol, potassium hexachloroiridate(III), and hexaamine ruthenium(III) chloride).

through the hydrogel film. Considerable amplification occurred when the NP samples were entrapped in the hydrogel film due to the redox cycling of the mediator with entrapped NPs, which amplifies the current signals. Significant differences between the two types of NPs were observed in the Ru^{3+} region. For PDA NPs (Figure 6A), enhanced reduction peaks were observed, while for the radical samples (Figure 6B), both reduction and oxidation peaks were enhanced. These results indicate that radical NPs are more reducing than conventional PDA and synthetic chemistry can be leveraged to tune the redox properties of these pigments, which is consistent with the ROS scavenging experiments described above.

CONCLUSIONS

In conclusion, we demonstrate a strategy for increasing radical content by chemically incorporating stable radicals into melanin-mimicking nanoparticles. This copolymerization route provides a methodology for preparing chemically functionalized melanin-mimics by a bottom-up approach. The resulting particles have different electrochemical and magnetic properties as compared with conventional polydopamine, enriching the current melanin library. The intrinsic EPR signal of this new melanin is different from any existing melanin materials. The radical-enriched melanin shows excellent uptake in keratinocyte cells and eliminates ROS from cells efficiently after X-ray irradiation. The concept of using optimized radical-enriched melanin NPs for radiation protection, accessible via this generalizable synthetic procedure, would be applicable in applications such as unwanted exposure during clinical radiation treatment.

ASSOCIATED CONTENT

Supporting Information

The Supporting Information is available free of charge at https://pubs.acs.org/doi/10.1021/acs.chemmater.0c01573.

Materials and instruments, detailed synthesis of monomer and radical NPs, ^{1}H NMR and ^{13}C NMR spectra, DLS, MS, EPR calibration curve, cytotoxicity, cell uptake study images, and single channel confocal images (PDF)

https://dx.doi.org/10.1021/acs.chemmater.0c01573
Chem. Mater. 2020, 32, 5759−5767

AUTHOR INFORMATION

Corresponding Authors

Jeffrey D. Rinehart − *Department of Chemistry and Biochemistry, University of California, San Diego, La Jolla, California 92093, United States;* orcid.org/0000-0002-5478-1995; Email: jrinehart@ucsd.edu

Nathan C. Gianneschi − *Department of Chemistry, Northwestern University, Evanston, Illinois 60208, United States; Chemistry of Life Processes Institute, Lurie Cancer Center, Northwestern University, Department of Biomedical Engineering, and International Institute of Nanotechnology, Evanston, Illinois 60208, United States;* orcid.org/0000-0001-9945-5475; Email: nathan.gianneschi@northwestern.edu

Authors

Wei Cao − *Department of Chemistry, Northwestern University, Evanston, Illinois 60208, United States; Chemistry of Life Processes Institute, Lurie Cancer Center, Northwestern University, Department of Biomedical Engineering, and International Institute of Nanotechnology, Evanston, Illinois 60208, United States;* orcid.org/0000-0002-5048-7991

Alex J. Mantanona − *Department of Chemistry and Biochemistry, University of California, San Diego, La Jolla, California 92093, United States*

Haochuan Mao − *Department of Chemistry, Northwestern University, Evanston, Illinois 60208, United States; Institute for Sustainability and Energy at Northwestern University, Evanston, Illinois 60208, United States;* orcid.org/0000-0001-8742-089X

Naneki C. McCallum − *Department of Chemistry, Northwestern University, Evanston, Illinois 60208, United States; Chemistry of Life Processes Institute, Lurie Cancer Center, Northwestern University, Department of Biomedical Engineering, and International Institute of Nanotechnology, Evanston, Illinois 60208, United States;* orcid.org/0000-0001-9210-3493

Yang Jiao − *Department of Chemistry, Northwestern University, Evanston, Illinois 60208, United States*

Claudia Battistella − *Department of Chemistry, Northwestern University, Evanston, Illinois 60208, United States; Chemistry of Life Processes Institute, Lurie Cancer Center, Northwestern University, Department of Biomedical Engineering, and International Institute of Nanotechnology, Evanston, Illinois 60208, United States*

Valeria Caponetti − *Dipartimento di Chimica "G. Ciamician", Università di Bologna, 40126 Bologna, Italy*

Nanzhi Zang − *Department of Chemistry, Northwestern University, Evanston, Illinois 60208, United States; Chemistry of Life Processes Institute, Lurie Cancer Center, Northwestern University, Department of Biomedical Engineering, and International Institute of Nanotechnology, Evanston, Illinois 60208, United States*

Matthew P. Thompson − *Department of Chemistry, Northwestern University, Evanston, Illinois 60208, United States; Chemistry of Life Processes Institute, Lurie Cancer Center, Northwestern University, Department of Biomedical Engineering, and International Institute of Nanotechnology, Evanston, Illinois 60208, United States*

Marco Montalti − *Dipartimento di Chimica "G. Ciamician", Università di Bologna, 40126 Bologna, Italy*

J. Fraser Stoddart − *Department of Chemistry, Northwestern University, Evanston, Illinois 60208, United States; Institute of Molecular Design and Synthesis, Tianjin University, Tianjin 300072, China; School of Chemistry, University of New South Wales, Sydney, New South Wales 2052, Australia;* orcid.org/0000-0003-3161-3697

Michael R. Wasielewski − *Department of Chemistry, Northwestern University, Evanston, Illinois 60208, United States; Institute for Sustainability and Energy at Northwestern University, Evanston, Illinois 60208, United States;* orcid.org/0000-0003-2920-5440

Complete contact information is available at: https://pubs.acs.org/10.1021/acs.chemmater.0c01573

Author Contributions

The manuscript was written through contributions of all authors. All authors have given approval to the final version of the manuscript.

Funding

This work was supported by a MURI grant through the Air Force Office of Scientific Research (no. FA9550-18-1-0142). EPR spectroscopy was supported by the National Science Foundation under award no. CHE-1900422 (M.R.W.). Y.J. and J.F.S. thank Northwestern University for their support to their contribution on this research project.

Notes

The authors declare no competing financial interest.

ACKNOWLEDGMENTS

The authors would like to thank Prof. Bethany Perez-White in the department of dermatology at the Northwestern Feinberg School of Medicine for the NHEK cells and her expertise in keratinocyte cell culture.

ABBREVIATIONS

NP, nanoparticle; PDA, polydopamine; EPR, electron paramagnetic resonance; NHEK, neonatal human epidermal keratinocytes; TEM, transmission electron microscopy; FTIR, Fourier-transform infrared; SQUID, superconducting quantum interference device; CV, cyclic voltammetry; ROS, reactive oxygen species; CLSM, confocal laser scanning microscopy; WGA, wheat germ agglutinin; DCFDA, 2′,7′, dichlorofluorescein diacetate; DHICA, 5,6-dihydroxyindole-2-carboxylic acid; DHI, 5,6-dihydroxyindole; HKGS, human keratinocyte growth supplement; DMEM, Dulbecco's modified Eagle medium; FBS, fetal bovine serum; PBS, phosphate-buffered saline

REFERENCES

(1) D'Alba, L.; Shawkey, M. D. Melanosomes: Biogenesis, Properties, and Evolution of an Ancient Organelle. *Physiol. Rev.* **2019**, *99*, 1−19.

(2) d'Ischia, M.; Napolitano, A.; Ball, V.; Chen, C. T.; Buehler, M. J. Polydopamine and eumelanin: from structure-property relationships to a unified tailoring strategy. *Acc. Chem. Res.* **2014**, *47*, 3541−3550.

(3) Ryu, J. H.; Messersmith, P. B.; Lee, H. Polydopamine Surface Chemistry: A Decade of Discovery. *ACS Appl. Mater. Interfaces* **2018**, *10*, 7523−7540.

(4) Lampel, A.; McPhee, S. A.; Park, H.-A.; Scott, G. G.; Humagain, S.; Hekstra, D. R.; Yoo, B.; Frederix, P. W. J. M.; Li, T.-D.; Abzalimov, R. R.; Greenbaum, S. G.; Tuttle, T.; Hu, C.; Bettinger, C. J.; Ulijn, R. V. Polymeric peptide pigments with sequence-encoded properties. *Science* **2017**, *356*, 1064−1068.

(5) Premi, S.; Wallisch, S.; Mano, C. M.; Weiner, A. B.; Bacchiocchi, A.; Wakamatsu, K.; Bechara, E. J. H.; Halaban, R.; Douki, T.; Brash,

D. E. Chemiexcitation of melanin derivatives induces DNA photoproducts long after UV exposure. *Science* **2015**, *347*, 842−847.
(6) Lee, H.; Dellatore, S. M.; Miller, W. M.; Messersmith, P. B. Mussel-Inspired Surface Chemistry for Multifunctional Coatings. *Science* **2007**, *318*, 426−430.
(7) Seagle, B.-L. L.; Rezai, K. A.; Kobori, Y.; Gasyna, E. M.; Rezaei, K. A.; Norris, J. R., Jr. Melanin photoprotection in the human retinal pigment epithelium and its correlation with light-induced cell apoptosis. *Proc. Nat. Acad. Sci. U. S. A.* **2005**, *102*, 8978−8983.
(8) Xiao, M.; Li, Y.; Zhao, J.; Wang, Z.; Gao, M.; Gianneschi, N. C.; Dhinojwala, A.; Shawkey, M. D. Stimuli-Responsive Structurally Colored Films from Bioinspired Synthetic Melanin Nanoparticles. *Chem. Mater.* **2016**, *28*, 5516−5521.
(9) Xiao, M.; Li, Y.; Allen, M. C.; Deheyn, D. D.; Yue, X.; Zhao, J.; Gianneschi, N. C.; Shawkey, M. D.; Dhinojwala, A. Bio-Inspired Structural Colors Produced *via* Self-Assembly of Synthetic Melanin Nanoparticles. *ACS Nano* **2015**, *9*, 5454−5460.
(10) Ju, K.-Y.; Lee, Y.; Lee, S.; Park, S. B.; Lee, J.-K. Bioinspired Polymerization of Dopamine to Generate Melanin-Like Nanoparticles Having an Excellent Free-Radical-Scavenging Property. *Biomacromolecules* **2011**, *12*, 625−632.
(11) Liu, Y.; Ai, K.; Ji, X.; Askhatova, D.; Du, R.; Lu, L.; Shi, J. Comprehensive Insights into the Multi-Antioxidative Mechanisms of Melanin Nanoparticles and Their Application To Protect Brain from Injury in Ischemic Stroke. *J. Am. Chem. Soc.* **2017**, *139*, 856−862.
(12) Huang, Y.; Li, Y.; Hu, Z.; Yue, X.; Proetto, M. T.; Jones, Y.; Gianneschi, N. C. Mimicking Melanosomes: Polydopamine Nanoparticles as Artificial Microparasols. *ACS Cent. Sci.* **2017**, *3*, 564−569.
(13) Slominski, A.; Tobin, D. J.; Shibahara, S.; Wortsman, J. Melanin pigmentation in mammalian skin and its hormonal regulation. *Physiol. Rev.* **2004**, *84*, 1155−1228.
(14) Zhao, H.; Zeng, Z.; Liu, L.; Chen, J.; Zhou, H.; Huang, L.; Huang, J.; Xu, H.; Xu, Y.; Chen, Z.; Wu, Y.; Guo, W.; Wang, J. H.; Wang, J.; Liu, Z. Polydopamine nanoparticles for the treatment of acute inflammation-induced injury. *Nanoscale* **2018**, *10*, 6981−6991.
(15) Liu, F.; He, X.; Zhang, J.; Chen, H.; Zhang, H.; Wang, Z. Controllable synthesis of polydopamine nanoparticles in microemulsions with pH-activatable properties for cancer detection and treatment. *J. Mater. Chem. B* **2015**, *3*, 6731−6739.
(16) Ito, S. A Chemist's View of Melanogenesis. *Anal. Biochem.* **2003**, *16*, 230−236.
(17) Blois, M. S.; Zahlan, A. B.; Maling, J. E. Electron Spin Resonance Studies on Melanin. *Biophys. J.* **1964**, *4*, 471−490.
(18) Mostert, A. B.; Rienecker, S. B.; Noble, C.; Hanson, G. R.; Meredith, P. The photoreactive free radical in eumelanin. *Sci. Adv.* **2018**, *4*, No. eaaq1293.
(19) Kang, X.; Cai, W.; Zhang, S.; Cui, S. Revealing the formation mechanism of insoluble polydopamine by using a simplified model system. *Polym. Chem* **2017**, *8*, 860−864.
(20) Sealy, R. C.; Hyde, J. S.; Felix, C. C.; Menon, I. A.; Prota, G. Eumelanins and pheomelanins: characterization by electron spin resonance spectroscopy. *Science* **1982**, *217*, 545−547.
(21) Nambiar, S.; Yeow, J. T. W. Polymer-composite materials for radiation protection. *ACS Appl. Mater. Interfaces* **2012**, *4*, 5717−5726.
(22) Moding, E. J.; Kastan, M. B.; Kirsch, D. G. Strategies for optimizing the response of cancer and normal tissues to radiation. *Nat. Rev. Drug Discovery* **2013**, *12*, 526−542.
(23) Cao, W.; Gu, Y.; Meineck, M.; Xu, H. The Combination of Chemotherapy and Radiotherapy towards More Efficient Drug Delivery. *Chem. − Asian J.* **2014**, *9*, 48−57.
(24) Fazel, R.; Krumholz, H. M.; Wang, Y.; Ross, J. S.; Chen, J.; Ting, H. H.; Shah, N. D.; Nasir, K.; Einstein, A. J.; Nallamothu, B. K. Exposure to Low-Dose Ionizing Radiation from Medical Imaging Procedures. *N. Engl. J. Med.* **2009**, *361*, 849−857.
(25) Weiss, J. F.; Landauer, M. R. Protection against ionizing radiation by antioxidant nutrients and phytochemicals. *Toxicology* **2003**, *189*, 1−20.
(26) Xu, C.; Tung, G. A.; Sun, S. Size and Concentration Effect of Gold Nanoparticles on X-ray Attenuation As Measured on Computed Tomography. *Chem. Mater.* **2008**, *20*, 4167−4169.
(27) Dadachova, E.; Bryan, R. A.; Howell, R. C.; Schweitzer, A. D.; Aisen, P.; Nosanchuk, J. D.; Casadevall, A. The radioprotective properties of fungal melanin are a function of its chemical composition, stable radical presence and spatial arrangement. *Pigm. Cell Melanoma Res.* **2008**, *21*, 192−199.
(28) Dadachova, E.; Bryan, R. A.; Huang, X.; Moadel, T.; Schweitzer, A. D.; Aisen, P.; Nosanchuk, J. D.; Casadevall, A. Ionizing radiation changes the electronic properties of melanin and enhances the growth of melanized fungi. *PLoS One* **2007**, *2*, No. e457.
(29) Zhou, X.; McCallum, N. C.; Hu, Z.; Cao, W.; Gnanasekaran, K.; Feng, Y.; Stoddart, J. F.; Wang, Z.; Gianneschi, N. C. Artificial Allomelanin Nanoparticles. *ACS Nano* **2019**, *13*, 10980−10990.
(30) Mironenko, N. V.; Alekhina, I. A.; Zhdanova, N. N.; Bulat, S. A. Intraspecific variation in gamma-radiation resistance and genomic structure in the filamentous fungus Alternaria alternata: a case study of strains inhabiting Chernobyl reactor no. 4. *Ecotoxicol. Environ. Saf.* **2000**, *45*, 177−187.
(31) Schweitzer, A. D.; Revskaya, E.; Chu, P.; Pazo, V.; Friedman, M.; Nosanchuk, J. D.; Cahill, S.; Frases, S.; Casadevall, A.; Dadachova, E. Melanin-covered nanoparticles for protection of bone marrow during radiation therapy of cancer. *Int. J. Radiat. Oncol., Biol., Phys.* **2010**, *78*, 1494−1502.
(32) Schweitzer, A. D.; Howell, R. C.; Jiang, Z.; Bryan, R. A.; Gerfen, G.; Chen, C. C.; Mah, D.; Cahill, S.; Casadevall, A.; Dadachova, E. Physico-chemical evaluation of rationally designed melanins as novel nature-inspired radioprotectors. *PLoS One* **2009**, *4*, No. e7229.
(33) Li, Y.; Xie, Y.; Wang, Z.; Zang, N.; Carniato, F.; Huang, Y.; Andolina, C. M.; Parent, L. R.; Ditri, T. B.; Walter, E. D.; Botta, M.; Rinehart, J. D.; Gianneschi, N. C. Structure and Function of Iron-Loaded Synthetic Melanin. *ACS Nano* **2016**, *10*, 10186−10194.
(34) Sarna, T.; Plonka, P. M. Biophysical Studies of Melanin. In *Biomedical EPR, Part A: Free Radicals, Metals, Medicine, and Physiology*, Eaton, S. R.; Eaton, G. R.; Berliner, L. J., Eds. Springer US: Boston, MA, 2005; pp 125−146.
(35) Sarna, T.; Lukiewicz, S. Electron spin resonance studies on living cells. IV. Pathological changes in amphibian eggs and embryos. *Folia Histochem. Cytochem.* **1972**, *10*, 265−278.
(36) Hansen, K.-A.; Blinco, J. P. Nitroxide radical polymers − a versatile material class for high-tech applications. *Polym. Chem.* **2018**, *9*, 1479−1516.
(37) Wilcox, C. S. Effects of tempol and redox-cycling nitroxides in models of oxidative stress. *Pharmacol. Ther.* **2010**, *126*, 119−145.
(38) Neil, S.; Huh, J.; Baronas, V.; Li, X.; McFarland, H. F.; Cherukuri, M.; Mitchell, J. B.; Quandt, J. A. Oral administration of the nitroxide radical TEMPOL exhibits immunomodulatory and therapeutic properties in multiple sclerosis models. *Brain, Behav., Immun.* **2017**, *62*, 332−343.
(39) Bain, G. A.; Berry, J. F. Diamagnetic Corrections and Pascal's Constants. *J. Chem. Educ.* **2008**, *85*, 532−536.
(40) Kim, E.; Panzella, L.; Micillo, R.; Bentley, W. E.; Napolitano, A.; Payne, G. F. Reverse Engineering Applied to Red Human Hair Pheomelanin Reveals Redox-Buffering as a Pro-Oxidant Mechanism. *Sci. Rep.* **2015**, *5*, 18447.
(41) Kang, M.; Kim, E.; Temoçin, Z.; Li, J.; Dadachova, E.; Wang, Z.; Panzella, L.; Napolitano, A.; Bentley, W. E.; Payne, G. F. Reverse Engineering To Characterize Redox Properties: Revealing Melanin's Redox Activity through Mediated Electrochemical Probing. *Chem. Mater.* **2018**, *30*, 5814−5826.
(42) Woehlk, H.; Steinkoenig, J.; Lang, C.; Michalek, L.; Trouillet, V.; Krolla, P.; Goldmann, A. S.; Barner, L.; Blinco, J. P.; Barner-Kowollik, C.; Fairfull-Smith, K. E. Engineering Nitroxide Functional Surfaces Using Bioinspired Adhesion. *Langmuir* **2018**, *34*, 3264−3274.
(43) Woehlk, H.; Trimble, M. J.; Mansour, S. C.; Pletzer, D.; Trouillet, V.; Welle, A.; Barner, L.; Hancock, R. E. W.; Barner-

Kowollik, C.; Fairfull-Smith, K. E. Controlling biofilm formation with nitroxide functional surfaces. *Polym. Chem.* **2019**, *10*, 4252−4258.
(44) Woehlk, H.; Lauer, A.; Trouillet, V.; Welle, A.; Barner, L.; Blinco, J. P.; Fairfull-Smith, K. E.; Barner-Kowollik, C. Dynamic Nitroxide Functional Materials. *Chem. − Eur. J.* **2018**, *24*, 18873−18879.
(45) Cao, Q.; Dornan, L. M.; Rogan, L.; Hughes, N. L.; Muldoon, M. J. Aerobic oxidation catalysis with stable radicals. *Chem. Commun.* **2014**, *50*, 4524−4543.
(46) Wang, X.; Chen, Z.; Yang, P.; Hu, J.; Wang, Z.; Li, Y. Size control synthesis of melanin-like polydopamine nanoparticles by tuning radicals. *Polym. Chem.* **2019**, *10*, 4194−4200.
(47) Hong, S.; Wang, Y.; Park, S. Y.; Lee, H. Progressive fuzzy cation-π assembly of biological catecholamines. *Sci. Adv.* **2018**, *4*, No. eaat7457.
(48) d'Ischia, M.; Napolitano, A.; Pezzella, A.; Meredith, P.; Buehler, M. Melanin Biopolymers: Tailoring Chemical Complexity for Materials Design. *Angew. Chem., Int. Ed.* **2020**, DOI: 10.1002/anie.201914276.
(49) Yang, P.; Gu, Z.; Zhu, F.; Li, Y. Structural and Functional Tailoring of Melanin-Like Polydopamine Radical Scavengers. *CCS Chem.* **2020**, *2*, 128−138.
(50) Pyo, J.; Ju, K. Y.; Lee, J. K. Artificial pheomelanin nanoparticles and their photo-sensitization properties. *J. Photochem. Photobiol., B* **2016**, *160*, 330−335.
(51) Chumakova, N. A.; Ivanova, T. A.; Golubeva, E. N.; Kokorin, A. I. To the Precision of Measuring Concentrations of Nitroxide Radicals in Polymers by EPR Technique. *Appl. Magn. Reson.* **2018**, *49*, 511−522.
(52) Wang, Z.; Xie, Y.; Li, Y.; Huang, Y.; Parent, L. R.; Ditri, T.; Zang, N.; Rinehart, J. D.; Gianneschi, N. C. Tunable, Metal-Loaded Polydopamine Nanoparticles Analyzed by Magnetometry. *Chem. Mater.* **2017**, *29*, 8195−8201.
(53) Badetti, E.; Lloveras, V.; Muñoz-Gómez, J. L.; Sebastián, R. M.; Caminade, A. M.; Majoral, J. P.; Veciana, J.; Vidal-Gancedo, J. Radical Dendrimers: A Family of Five Generations of Phosphorus Dendrimers Functionalized with TEMPO Radicals. *Macromolecules* **2014**, *47*, 7717−7724.
(54) Ando, H.; Niki, Y.; Ito, M.; Akiyama, K.; Matsui, M. S.; Yarosh, D. B.; Ichihashi, M. Melanosomes Are Transferred from Melanocytes to Keratinocytes through the Processes of Packaging, Release, Uptake, and Dispersion. *J. Invest. Dermatol.* **2012**, *132*, 1222−1229.
(55) National Research Council *Committee on the Biological Effects of Ionizing, R., Health Effects of Exposure to Low Levels of Ionizing Radiation : BEIR V*; National Academies: 2001.
(56) Korystov, Y. N.; Shaposhnikova, V. V.; Korystova, A. F.; Emel'yanov, M. O. Detection of Reactive Oxygen Species Induced by Radiation in Cells Using the Dichlorofluorescein Assay. *Radiat. Res.* **2007**, *168*, 226−232.
(57) Leach, J. K.; Van Tuyle, G.; Lin, P.-S.; Schmidt-Ullrich, R.; Mikkelsen, R. B. Ionizing Radiation-induced, Mitochondria-dependent Generation of Reactive Oxygen/Nitrogen. *Cancer Res.* **2001**, *61*, 3894−3901.

https://dx.doi.org/10.1021/acs.chemmater.0c01573
Chem. Mater. 2020, 32, 5759−5767